Proximity exchange coupling in a Fe/MgO/Si tunnel contact detected by the inverted Hanle effect

R. Jansen,[1] A. Spiesser,[1] H. Saito,[1] Y. Fujita,[1] S. Yamada,[2] K. Hamaya,[2] and S. Yuasa[1]

[1]*Spintronics Research Center, National Institute of Advanced Industrial Science and Technology (AIST), Tsukuba, Ibaraki, 305-8568, Japan*

[2]*Center for Spintronics Research Network, Graduate School of Engineering Science, Osaka University, Toyonaka 560-8531, Japan*

(Received 29 July 2019; revised manuscript received 11 September 2019; published 26 November 2019)

A ferromagnet is shown to exert an exchange field on the spin accumulation localized in the semiconductor interface region of a Fe/MgO/Si tunnel contact. The proximity exchange coupling across the MgO modifies spin precession of the spin accumulation and thereby produces detectable signatures in the inverted Hanle effect: exchange-induced shifts of the inverted Hanle curves, hysteresis, and discontinuities at the coercive field of the ferromagnet, at which the exchange field is reversed. The proximity exchange field is locked antiparallel to the magnetization of the ferromagnet, has values up to 380 Oe, and can be controlled by a bias voltage across the tunnel contact.

DOI: 10.1103/PhysRevB.100.174432

I. INTRODUCTION

At an interface between a ferromagnet and a nonferromagnetic material, the ferromagnet (FM) induces a proximity exchange field inside the nonmagnetic (NM) material, which creates a net nonzero magnetization in the NM material. The proximity exchange field has a particularly strong effect for nonmagnetic materials that are close to being ferromagnetic, such as platinum and palladium. Unfortunately, the interaction is short range and the induced magnetization is therefore confined to the first few layers of atoms directly adjacent to the interface. Interestingly, the recent advances [1–6] in the use of two-dimensional (2D) materials, such as graphene and van der Waals heterostructures, in spintronic devices create new opportunities to employ proximity effects efficiently [7,8] since the proximity exchange field extends over the full depth of such 2D materials. Indeed, the presence of a proximity-induced magnetic exchange field was recently observed in graphene and other monolayer materials in contact with a ferromagnet [9–11].

Although the proximity exchange field turns a nonmagnetic material into an equilibrium ferromagnet, the net magnetization is rather small. For instance, an exchange field of 1 T corresponds to a spin splitting of $\sim$100 μeV in materials with an electron g factor equal to 2. A much larger spin splitting, albeit nonequilibrium, can be induced in NM materials by spin injection from a FM tunnel contact using an electrical current. With this method spin accumulations in the range of 1–10 meV have been obtained in materials such as graphene [12,13] and silicon [14–16]. Proximity exchange fields larger than 1 T are possible [9] with strongly ferromagnetic EuS, albeit at low temperature. Nonetheless, an alternative and perhaps more viable approach is to use the proximity exchange field for the dynamic manipulation of spins in a NM material [8,10,17]. The spin precession [18,19] in a magnetic field perpendicular to the spins in a NM material (Hanle effect) requires a field for which $\omega\tau_s$ is of the order of 1, where ω is the Larmor frequency and τ_s the spin-relaxation time. For materials with a spin lifetime in the 1–10 ns range, the relevant magnetic fields are in the 10–1 mT range. Effective fields of such a small magnitude can readily be produced by a proximity exchange interaction. Indeed, the relatively small exchange field (of about 0.2 T) in single-layer graphene placed on a ferromagnetic insulator substrate (yttrium iron garnet, YIG) was detected via the changes in the Hanle spin precession of the spin accumulation in the graphene [10], rather than detecting the minute magnetization or spin splitting induced by the exchange field.

Instead of a direct contact between the FM and the NM materials, exchange coupling can also occur across a tunneling barrier, as pointed out by Slonczewski [20] for a magnetic tunnel junction consisting of two ferromagnets separated by a tunneling barrier. Exchange via tunneling has been observed in crystalline MgO-based magnetic tunnel junctions [21–23]. The exchange coupling, mediated by tunnel electrons, should be distinguished from magnetic interlayer coupling of magnetostatic origin (either the so-called Néel "orange-peel" coupling [24,25], between two ferromagnets across the tunnel barrier due to magnetostatic dipolar fields arising from the finite interface roughness, or the antiferromagnetic coupling arising from lateral flux closure of the stray fields between the magnetic layers outside the area of the tunnel junction, which depends on the lateral size and the aspect ratio of the tunnel contact [26]). Although exchange coupling via tunneling electrons is expected to be relatively small owing to the presence of the tunnel barrier, as pointed out above, even small exchange fields may be sufficient to manipulate a spin accumulation in a nonmagnetic material, particularly for materials with large τ_s.

Here, we therefore explore exchange coupling across an MgO tunnel barrier in a Fe/MgO/Si structure. It is shown that the ferromagnetic Fe exerts an exchange field on the spin accumulation localized in the semiconductor interface region of the Fe/MgO/Si tunnel contact. The proximity exchange coupling across the MgO modifies spin precession of the interface spin accumulation and thereby produces detectable signatures in the inverted Hanle effect: exchange-induced shifts of the inverted Hanle curves, hysteresis, and

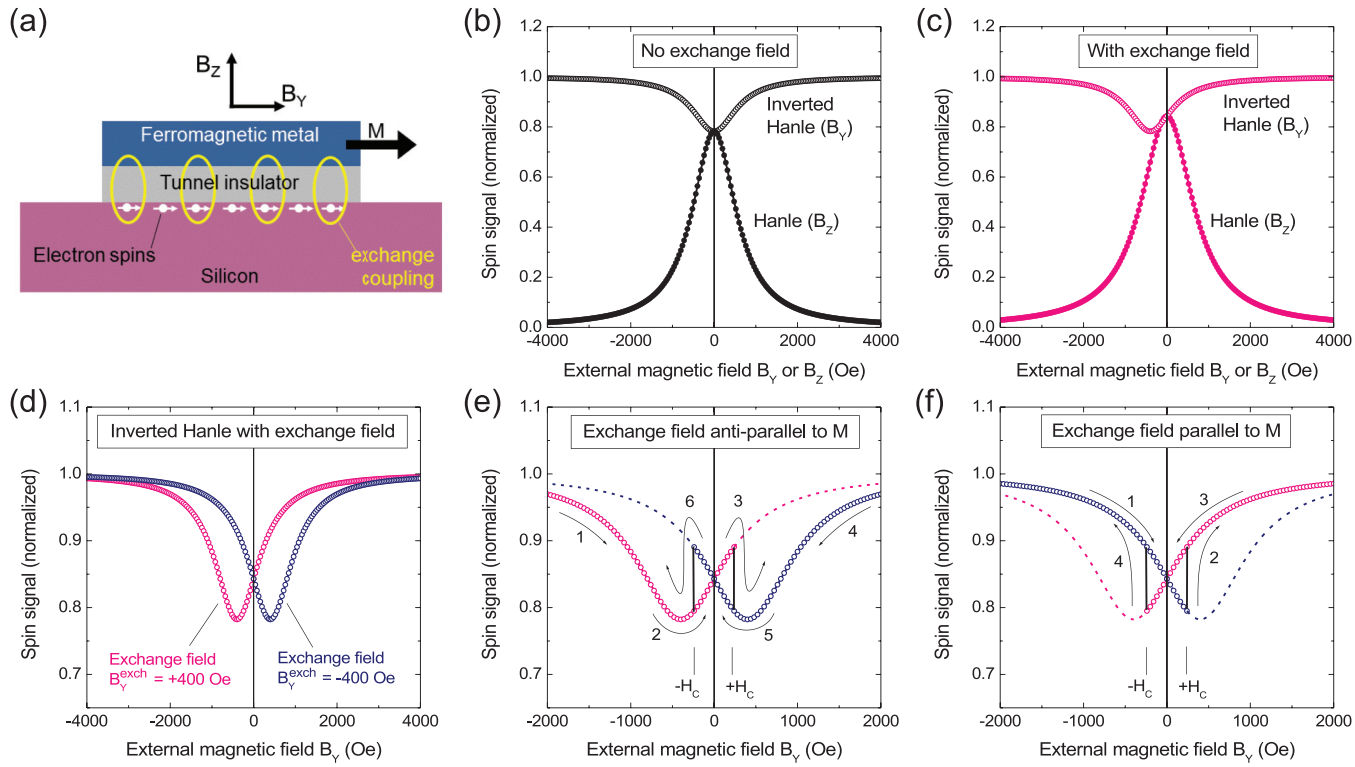

FIG. 1. Simulation of the effect of an exchange field on the inverted Hanle curves. (a) Schematic illustration of exchange coupling across a FM/insulator/Si tunnel contact. The yellow ellipses denote the exchange coupling. The magnetization M, the exchange field, and the spins at the Si interface point parallel to the tunnel interface. (b) Calculated Hanle and inverted Hanle curves in the absence of exchange fields. The spin lifetime was set to 100 ps and the inverted Hanle effect was induced by including a magnetostatic (stray) field of 300 Oe in the x direction, which is orthogonal to the polarization direction of the spins (y direction). The external field points along the z or the y direction for the Hanle and inverted Hanle curves, respectively. (c) Similar calculation, but now with a constant exchange field of +400 Oe in the y direction. (d) Calculated inverted Hanle curves for a constant exchange field of +400 Oe (pink curve) or −400 Oe (blue curve) in the y direction. (e), (f) Simulated inverted Hanle curves which take into account the sign reversal of the exchange field at the coercive fields ($\pm H_C$) of the ferromagnet, leading to the discontinuities indicated by the black solid lines. The magnetic field is swept from minus to plus and then back, with an exchange field of 400 Oe that is locked either antiparallel (e) or parallel (f) to the magnetization of the ferromagnet, which is oriented along the y axis.

discontinuities at the coercive field of the ferromagnet, at which the exchange field is reversed. The proximity exchange field is locked antiparallel to the magnetization of the ferromagnet, has values up to 380 Oe (38 mT), and can be controlled by a bias voltage across the tunnel contact.

II. THEORY

Spin precession [18,19] of a nonequilibrium spin accumulation in a NM material is governed by the total magnetic field, which is the vector sum of the external applied magnetic field B^{ext} and any other, so-called internal magnetic fields B^{int}. The latter includes effective fields due to exchange coupling B^{exch}, as relevant here, but also magnetostatic (stray) fields B^{ms}, for example, those close to the interface of a ferromagnet with finite roughness. The latter fields are known to produce an inverted Hanle effect [27]. For a spin accumulation induced by electrical spin injection from a FM contact whose magnetization M is pointing along the y direction [Fig. 1(a)], the spin density in the NM material is described by the following general expression [27]:

$$S_y = S_0 \left\{ \frac{\omega_y^2}{\omega_L^2} + \left(\frac{\omega_x^2 + \omega_z^2}{\omega_L^2} \right) \left(\frac{1}{1 + (\omega_L \tau_s)^2} \right) \right\} \qquad (1)$$

with S_y the spin density pointing along the y direction, S_0 the spin density in the absence of any magnetic fields, and τ_s the spin-relaxation time. The Larmor frequency is given by $(\omega_x, \omega_y, \omega_z) = (g\mu_B/\hbar)(B_x, B_y, B_z)$, where g is the Landé g factor, μ_B is the Bohr magneton, $\hbar$ is Planck's constant divided by 2π, and $\omega_L^2 = \omega_x^2 + \omega_y^2 + \omega_z^2$. The components B_i of the magnetic field include external as well as internal fields (i.e., $B_i = B_i^{\text{ext}} + B_i^{\text{ms}} + B_i^{\text{exch}}$).

We simulate the effect of an exchange field using Eq. (1). In the absence of any exchange fields, the Hanle and inverted Hanle curves have the usual shape [Fig. 1(b)]. In the Hanle effect, an external field B_z perpendicular to the spins causes spin precession and a gradual decrease of the spin density to zero as the strength of the field increases. In the inverted Hanle effect, the external magnetic field is applied along the y direction, parallel to the spins. By itself, this has no effect. However, as shown previously [27], if the spins reside close to an interface with a ferromagnet with finite roughness, magnetostatic stray fields with components orthogonal to the spins are present. We simulate this by adding a constant stray field ($B_x^{\text{ms}} = 300$ Oe) in the x direction. At zero external field, the spin density is reduced by spin precession in the stray field. The spin density recovers as the external field increases

because this rotates the total magnetic field (vector sum of external and stray field) toward the y axis parallel to the spins, so that spin precession is suppressed [27]. Most importantly, the minimum of the inverted Hanle curve occurs when the external field is zero.

Let us now add an exchange field B_y^{exch} collinear with the magnetization M of the ferromagnet (y direction). The salient effect is to shift the inverted Hanle curve along the magnetic field axis [Fig. 1(c)]. The minimum of the inverted Hanle curve now occurs at a nonzero value of the external field, for which the sum of the external field and the exchange field is zero. Moreover, the direction of the shift is determined by the sign of the exchange field [Fig. 1(d)]. Hence, the magnitude and the sign of the exchange field can be obtained from the shift of the inverted Hanle curves. Note that for an exchange field along the y direction, there is no shift in the regular Hanle curve [Fig. 1(c)] obtained with a perpendicular field B_z, although there is some broadening.

So far, the exchange field was taken to be a constant. In reality, the exchange field is expected to be locked to the magnetization direction of the ferromagnet, and thus the exchange field will change sign when the magnetization reverses at the coercive field H_C. Therefore, the shift direction of the inverted Hanle curve is also reversed, producing a discontinuity in the inverted Hanle curve at the coercive field, as well as magnetic hysteresis in the inverted Hanle effect. The exact shape of the inverted Hanle curves then depends on whether the exchange field is locked parallel or antiparallel to the magnetization of the ferromagnet. Let us consider the antiparallel case first [Fig. 1(e)]. Starting at large negative external field, M points along $-y$, and thus the exchange field points along $+y$. The minimum of the inverted Hanle curve thus occurs at negative fields [pink curve in Fig. 1(e)]. As the external field is swept from minus to plus, we thus have a minimum *before* the external field reaches zero. When the external field reaches $+H_C$, the M and the exchange field change sign, and an abrupt jump of the spin density occurs since now M points along $+y$, the exchange field points along $-y$, and thus the inverted Hanle curve is shifted to the plus direction [blue curve in Fig. 1(e)]. A similar discontinuity occurs when the field is swept in the opposite direction, but due to hysteresis the discontinuity occurs at $-H_C$. The characteristic shape of the curves is distinctly different when the exchange field is locked parallel to M [see Fig. 1(f)]. In this case, starting at large negative external field, both M and the exchange field point along $-y$, and the minimum of the inverted Hanle curve occur *after* the external field has passed through zero [Fig. 1(f), blue curve]. Hence, from the inverted Hanle curves we can not only obtain the magnitude of the exchange field, but we can also infer whether the exchange field is parallel or antiparallel to M.

III. RESULTS

The experiments were performed on crystalline Fe/MgO contacts grown by molecular beam epitaxy onto a Si(001) substrate that contains a 70-nm-thick heavily doped n-type Si layer (carrier density 2.7×10^{19} cm^{-3} at 10 K). The MgO tunnel barrier is 2 nm thick and the Fe/MgO contacts are

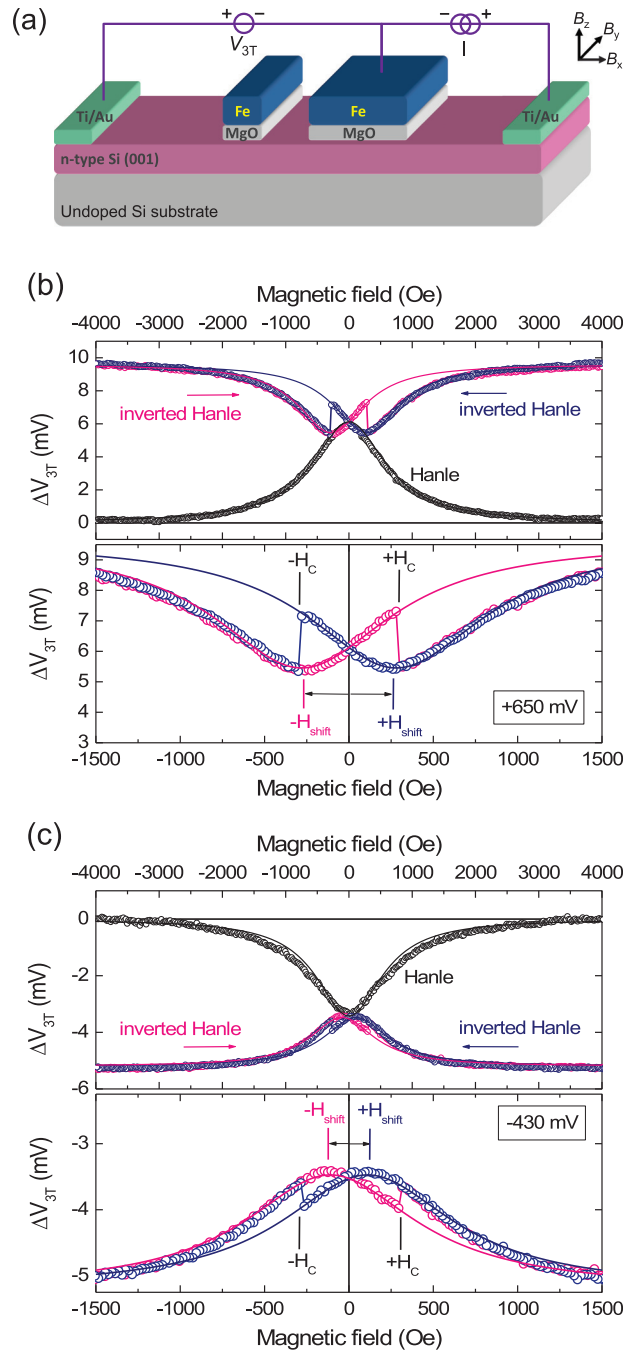

FIG. 2. Observation of the exchange field in a Fe/MgO/Si tunnel contact. (a) Device layout and measurement configuration. (b) Inverted Hanle data for a 0.4-μm-wide Fe/MgO contact at a bias voltage of +650 mV (+0.11 mA). The external field is in-plane (y direction) and swept from minus to plus (pink) or from plus to minus (dark blue). The Hanle curve obtained with an out-of-plane magnetic field (B_z) is also shown (black). An expanded view of the inverted Hanle curves is also included, with the exchange-induced shifts (H_{shift}) and the discontinuities at the coercive field (H_C) of the ferromagnet indicated. Solid lines are the corresponding fits using Eq. (1) (see text for further details). (c) Similar set of data for a bias voltage of −430 mV (−0.11 mA). The spin-independent part of the three-terminal voltage [+650 mV for (b) and −430 mV for (c)] that is due the nonzero tunnel current was subtracted. $T = 10$ K.

patterned into strips with a length of 40 μm along the y direction and four different widths along the x direction, respectively, 0.4, 0.8, 1.2, and 2.4 μm. The fabrication and characterization of the tunnel contacts have been described before, as they are part of the nonlocal spin-transport devices that we previously used to established that a giant spin accumulation can be created in the Si channel [14]. From the nonlocal spin-transport data we also extracted a large tunnel spin polarization of ∼53% at 10 K for the Fe/MgO tunnel contacts [14,15]. All data were obtained at a temperature (T) of 10 K.

For the experiments reported here, we use a single Fe/MgO contact and two nonmagnetic reference contacts in a three-terminal (3T) measurement configuration [28,29] [see Fig. 1(a)], and probe the spins using the Hanle and inverted Hanle effects [27]. The Hanle curve obtained with the external field along the z direction, perpendicular to the spins, is rather broad [Figs. 2(b) and 2(c)]. The linewidth is far from the 10–20 Oe that is expected for delocalized electrons in the Si channel, for which we previously determined a spin lifetime of 18 ns from nonlocal measurements in the same devices (see Appendix A). The observed broad Hanle curve therefore corresponds to spins that are trapped in the MgO/Si interface region, either in interface states or in the depletion region that is a few nm wide for heavily doped Si (see Appendix A for more details). The inverted Hanle curves, obtained with the external field applied along the y direction, are equally broad [Figs. 2(b) and 2(c)]. Therefore, these 3T Hanle and inverted Hanle curves, and any effects of the exchange field thereon, pertain electrons that are localized in the MgO/Si interface region, rather than delocalized electrons in the Si channel.

The salient features of the inverted Hanle curves are as follows. The curves are not centered around zero but shifted along the magnetic field axis. When the external field is swept from minus to plus, the minimum of the inverted Hanle curve occurs at a nonzero negative field [Figs. 2(b) and 2(c), pink curves], whereas the minimum occurs at a positive field when the external field is swept in the opposite direction (blue curves). Second, sharp jumps in the signal are observed at +290 Oe and −290 Oe. These values match the coercive field of the 0.4-μm-wide Fe/MgO contact, which we previously determined from nonlocal spin-valve measurements on the exact same tunnel contact [14]. Hence, the discontinuities occur when the magnetization of the Fe is reversed. These salient features are in perfect agreement with the simulations presented in Fig. 1(e). We thus conclude that (i) the Fe exerts an exchange field on the spins at the MgO/Si interface, (ii) the exchange field changes sign when the magnetization of the Fe reverses, and (iii) the exchange field is locked antiparallel to M [since the minimum of the inverted Hanle curves occurs before the field passes through zero, conforming with Fig. 1(e)]. Note that for perpendicular applied fields (Hanle configuration), a shift is not observed (the measured Hanle curve is centered at zero field and nonhysteretic). This implies that the exchange field does not have a perpendicular component and is thus collinear with M. Also note that the data cannot be explained by magnetostatic fields only, without an exchange field, as shown in Appendix B.

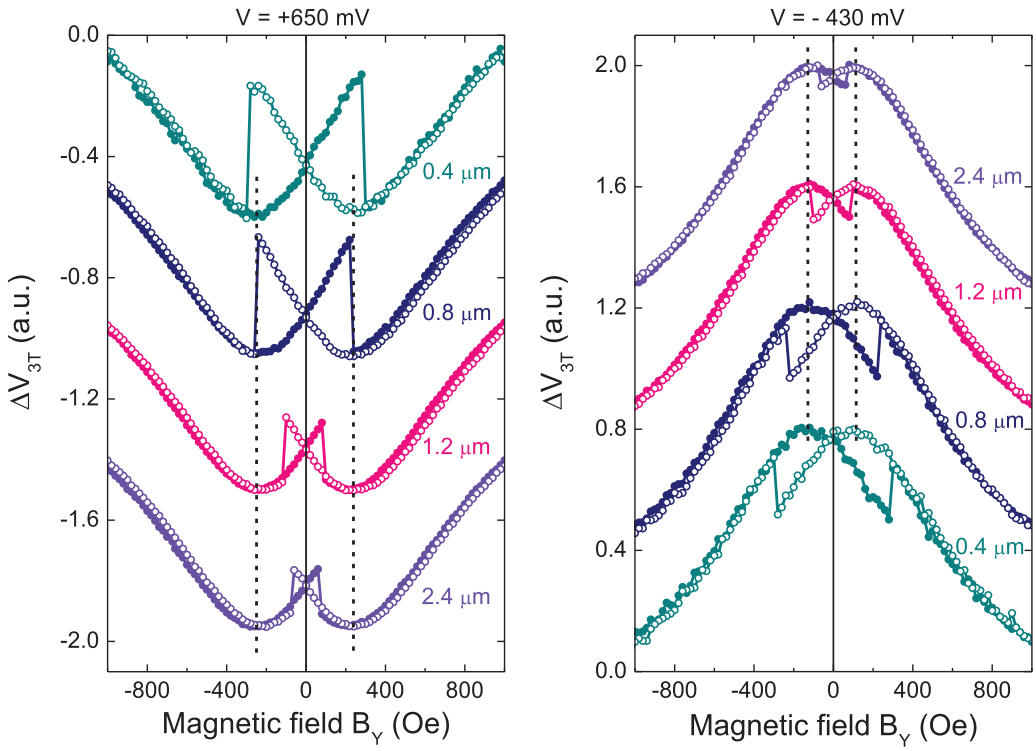

FIG. 3. Inverted Hanle data for Fe/MgO contacts of 40-μm length and different widths, respectively, 0.4, 0.8, 1.2, and 2.4 μm, as indicated. Data are shown for bias voltages of +650 mV (left panel) and −430 mV (right panel). The field is swept from minus to plus (solid symbols) and then back (open symbols). The dashed black lines indicate the position of the minimum or maximum of the inverted Hanle curves, which are shifted away from zero by the exchange field. $T = 10$ K.

When we compare the inverted Hanle curves for different bias voltage [Figs. 2(b) and 2(c)], we first of all note that the discontinuities occur at the same fields. This is expected if indeed the discontinuities are associated with the reversal of the magnetization of the Fe. To corroborate this, we performed similar inverted Hanle measurements on contact strips having different widths and therefore different coercive fields (Fig. 3). From the nonlocal spin-valve measurements performed previously on the same devices [14], we determine the values of the H_C to be 290, 230, 110, and 75 Oe, respectively, for the contacts of width 0.4, 0.8, 1.2, and 2.4 μm. The discontinuities in the inverted Hanle curves are indeed found to occur at smaller fields as the contact width is increased (Fig. 3), and the position of the discontinuities matches very well with the values of H_C for each of the contacts. This proves unambiguously that the discontinuity is associated with the magnetization reversal at $\pm H_C$.

The data in Fig. 3 also reveal that the *minimum* of the inverted Hanle curves, as indicated by the dashed black lines, does *not* depend on the width of the contact. This is as it should be since the magnitude of the exchange field is expected to be controlled by the tunneling process, rather than the shape and size of the tunnel contact. Importantly, it can also be seen that the position of the minimum does depend on the bias voltage across the structure (i.e., the minimum occurs around $\pm$250 Oe for a bias voltage of +650 mV, and around $\pm$110 Oe for a bias voltage of $-$430 mV). To investigate this further, we measured the inverted Hanle signals on the 0.4-μm-wide contact at various bias voltages (Fig. 4). We observe that the position of the minimum changes systematically as a function of the bias voltage. The H_{shift} is almost +400 Oe at large positive bias (corresponding to injection of electrons from the Fe into the Si), decreases to about +200 Oe around zero bias, and is further reduced for larger negative bias. The shift of the Hanle curves and the discontinuities at H_C completely disappear at very large negative bias. These results suggest that there is a static exchange field of around +200 Oe in the absence of a tunnel current, as well as a contribution to the exchange field that is controlled by the bias voltage across the tunnel contact. This is in line with the predictions made by Slonczewski [20], who showed that there is an equilibrium exchange interaction across a tunnel barrier in the absence of a net tunnel current, as well as a dynamic contribution in the presence of a nonzero tunnel current.

The exchange interaction is facilitated by the overlap of the wave functions of the two electrodes (e.g., Fe and Si) in the tunnel barrier. In a magnetic tunnel contact, the tunnel spin polarization is known to depend on the bias voltage across the tunnel barrier. This is because at different bias voltage, different electronic states with different energy (below or above the Fermi energy) and different spin polarization control the tunneling current. It is then easy to understand that the exchange field should also depend on the bias voltage because the wave functions that determine the exchange coupling change with voltage. For our Fe/MgO-based tunnel contacts on Si, in which coherent tunneling and symmetry-based spin filtering occurs [16], a free-electron description of tunneling is not appropriate. Hence, a quantitative comparison with the theory for tunneling exchange by Slonczewski [20] cannot be made.

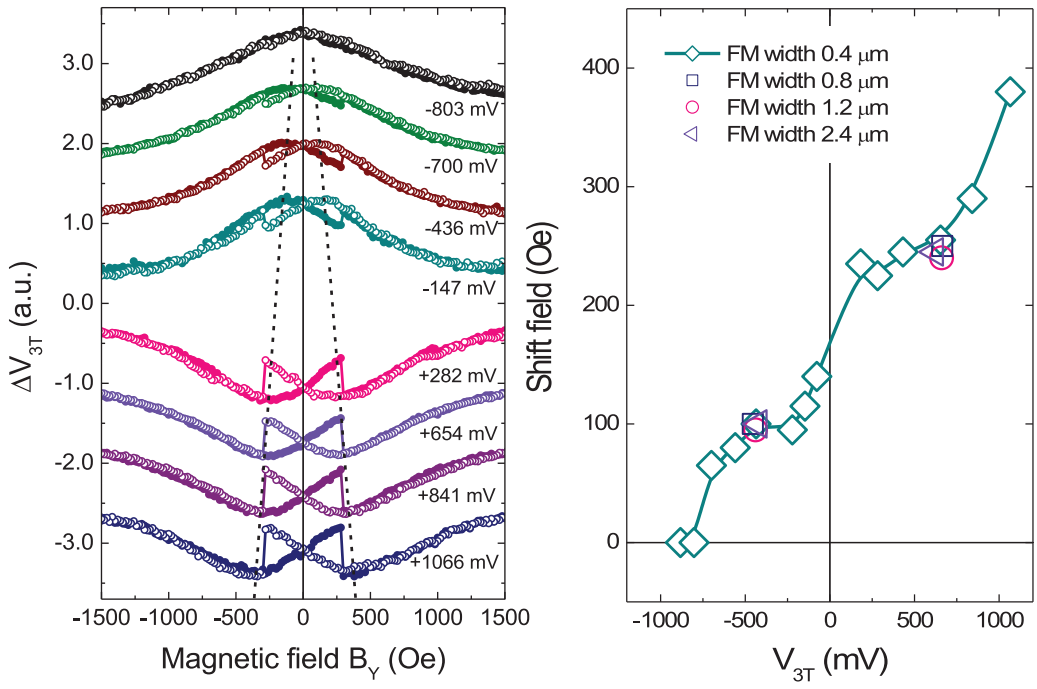

FIG. 4. Bias control of the exchange field. Left panel: Inverted Hanle data for a Fe/MgO contact of 0.4-μm width at different bias voltages, as indicated. The field is swept from minus to plus (solid symbols) and then back (open symbols). The voltage is obtained from a three-terminal measurement. The dashed black lines indicate the position of the minimum or maximum of the inverted Hanle curves, which are shifted away from zero magnetic field by an amount that depends on the bias voltage. $T = 10$ K. Right panel: The exchange field, extracted from the shifts of the inverted Hanle curves, as a function of the bias voltage.

IV. DISCUSSION

An exchange field of 400 Oe (≡40 mT) corresponds to a spin splitting of about 5 μeV, which is difficult to observe directly. For comparison, the spin accumulation induced by electrical spin injection from a current can be in the meV range [14,16], and thus much larger. In this regard one should keep in mind that the exchange-induced spin splitting is not a spin accumulation. The exchange shifts the energy of the electronic states up or down depending on the spin, but the electrochemical potential does not develop a spin splitting (conforming with a regular ferromagnet). Therefore, unlike a spin accumulation, the exchange-induced spin splitting cannot be detected by a Hanle measurement. But, as noted in the Introduction, if one introduces a spin accumulation by electrical spin injection, then even a small exchange field can have pronounced effects on the precession of the spin accumulation, enabling the easy detection of the exchange field via the (inverted) Hanle effect.

The exchange interaction across a tunnel barrier is expected to be rather weak because the electron wave functions decay exponentially into the tunnel barrier. The exchange field observed here reaches values close to 40 mT. This is not unreasonable considering that the effective exchange fields inside transition metal ferromagnets such as Fe are huge and of the order the 10^4 T (the exchange splitting in bulk transition metal ferromagnets is of order 1 eV). It is thus not inconceivable that a sizable exchange field still exists in proximity to the ferromagnet within a few nm distance, even if the decay is exponential. Indeed, the exchange fields deduced from our experiments are more than 10^5 times smaller than the exchange field in bulk Fe. Interlayer exchange interactions have also been observed in Fe/MgO superlattices [30,31] with MgO thicknesses (1.6 to 2.2 nm) comparable to that used in our Fe/MgO/Si devices (2 nm). Also, dynamic exchange coupling from a ferromagnet to localized states in CoFeB/MgO/Si structures was shown to play a role in spin pumping across the MgO tunnel barrier [32]. Localized states in the MgO/Si interface region are in close proximity to the FM (few nm), which may explain why a sizable exchange field is observed. The situation is quite similar to exchange fields induced in 2D materials such as graphene, which owing to their atomic-size thickness are within the range of the exchange interaction of the FM. Note that in the experiments [10] with graphene in contact with YIG, the ferromagnet was used as the substrate and thus induces an exchange field everywhere in the graphene layer. In contrast, the exchange coupling we report here exists in the tunnel contact area only and is confined to the MgO/Si interface. Indeed, in nonlocal spin-transport measurements in the same devices [14–16], we have not been able to detect any effect of the exchange coupling in the nonlocal spin signal since this is produced by the spin diffusion of delocalized electrons over lateral distances of the order of a micron through the 70-nm-thick Si channel.

Let us discuss the relation between the observations reported here and what is available in the literature on the inverted Hanle effect. Reexamining the first report of the inverted Hanle effect [27] reveals that the inverted Hanle curves reported there are distorted around zero external field. Although no hysteresis was observed, the distortions resemble what is reported here and, in retrospect, these features are also explained by the exchange field. The absence of hysteresis is because in that first report [27], contacts of large lateral size (∼100 μm in both directions) were used, and so the coercivity is much smaller than for contacts having a width of the order of a μm, as used here. As can be seen in Fig. 3, when the contact width increases and the coercivity decreases, the discontinuities in the inverted Hanle curve become smaller because they occur very close to zero field. In most other reports on the inverted Hanle effect, the curves are very similar to those in Ref. [27]. There are two exceptions. In a previous report using ferromagnetic Mn_5Ge_3 contacts on Ge [33], hysteresis and shifts of the inverted Hanle curves were observed. Although this may have been due to an exchange field, it is difficult to conclude this unambiguously because the magnetization reversal of the ferromagnetic contacts was not sharp. The features may therefore be due to the stray fields produced by the nonuniform magnetization during the magnetization reversal, which causes depolarization of the spins. Last but not least, features very similar to what we observe here have been reported in Ref. [34]. Although the authors gave a different interpretation, based on our current data, we conclude that exchange fields are also the origin of the features observed in Ref. [34] (see Appendix B for details).

As shown here, the exchange field produces easily detectable signatures in the inverted Hanle effect. This includes a shift of the inverted Hanle curve along the magnetic field axis because the exchange field and the external field point along the same axis (for the inverted Hanle effect, the field is applied parallel to the spins and thus to the magnetization of the ferromagnet, and the exchange field is also collinear with the magnetization of the ferromagnet, as observed here and previously [10]). In contrast, for the regular Hanle effect, the signatures of the exchange field are harder to discern because no shifts are produced when the exchange field is orthogonal to the external field. Although some broadening does occur for the regular Hanle effect, extracting the magnitude of the exchange field is not as straightforward. It should be noted that shifts of the regular Hanle curves can be produced if the exchange field is perpendicular to the spins, and thus collinear with the external field for the Hanle effect. This situation can be achieved if two different ferromagnets are used to produce the spin accumulation and the exchange field, respectively, and the two ferromagnets have orthogonal magnetization, as recently reported [17,35].

V. SUMMARY

It was shown that a ferromagnet exerts an exchange field on a nonequilibrium spin accumulation localized in the semiconductor at the tunnel interface of a Fe/MgO/Si junction. The exchange interaction modifies spin precession, producing shifts of the inverted Hanle curves, hysteresis, as well as discontinuities at the coercive field of the ferromagnet, at which the magnetization and thereby the exchange field changes sign. The exchange field reaches values close to 400 Oe and is found to be locked antiparallel to the magnetization of the ferromagnet. The magnitude of the exchange field is controlled by the bias voltage across the tunnel contact.

ACKNOWLEDGMENTS

This work was supported by the Grant-in-Aid for Scientific Research on Innovative Areas, "Nano Spin Conversion Science" (Grants No. 26103002 and No. 26103003), and by the Grant-in-Aid for Scientific Research (Grant No. 18K13807).

APPENDIX A

As described in the main text, the Hanle and inverted Hanle curves are rather broad (Fig. 2) and the linewidth (600–800 Oe) does not match with what is expected for delocalized electrons in the Si channel [36–38]. For the latter, a spin lifetime of 18 ns was previously determined from nonlocal spin-transport measurements in the same devices [14]. A linewidth of the order of 10 Oe is therefore expected for the 3T Hanle signal produced by spin accumulation of delocalized electrons in the channel. As can be seen in Fig. 5, the 3T Hanle curve for the Fe/MgO/Si contacts consists of a superposition of two Hanle peaks: A broad one that extends over several 1000 Oe, and a very sharp one that has a width of about 8 Oe. Importantly, the sharp Hanle peak has a linewidth that matches very well with what is calculated (using the previously described method [14]) for the spin accumulation of delocalized electrons in the Si channel with $\tau_s = 18$ ns and a contact width of 0.4 μm. The other, much broader, Hanle curve corresponds to spins that are trapped in the MgO/Si interface region, either in interface states [39,40] or, as the most recent experiments suggest [33], in the few-nm-wide depletion region of the heavily doped Si. Because the volume occupied by the localized states is much smaller than the volume of the Si channel, the spin accumulation in the localized states is much larger than that in the Si channel [39]. Moreover, the Hanle linewidth is not given by the spin lifetime but determined by an effective time constant that corresponds to the average time that the electrons dwell in the localized states before escaping [39,41]. It should thus be kept in mind that the broad 3T Hanle and inverted Hanle curves, and the effects of the exchange field thereon described in this paper, pertain spins that are localized in the MgO/Si interface region. These spins do not contribute to the spin signal observed in nonlocal spin-transport devices, which is produced by spin diffusion of delocalized electrons in the Si channel over lateral distances of the order of a micrometer.

Note that the sharp Hanle signal from delocalized electrons in the Si channel is observed for negative bias (extraction of spins from the Si), but is usually absent or very small for positive bias. This is due to the nonlinearity of spin detection, as recently explained [15]. Also note that for the data in Fig. 2(c), which were taken at negative bias, a sharp Hanle peak is absent because (i) the current is smaller (−0.11 mA), so that the spin accumulation in the channel is a factor of 6 smaller than for the data in Fig. 5, and (ii) the Hanle curve displayed in Fig. 2(c) was measured using a field sweep with a relatively large step size (20 Oe) so as to reduce the measurement time. The sharp Hanle peak is then not resolved.

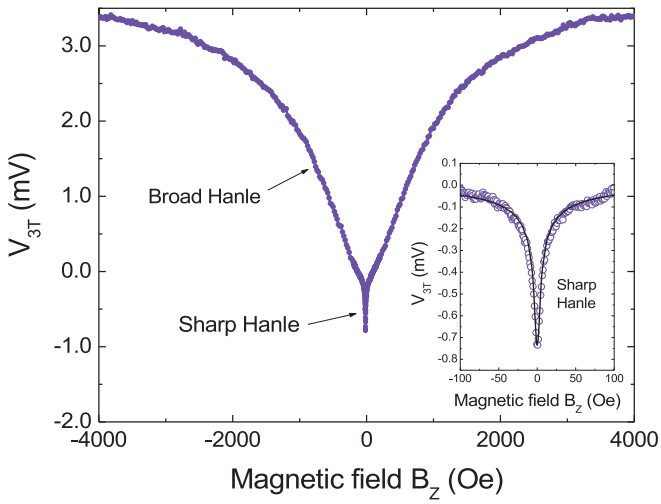

FIG. 5. Hanle spin signal measured in a three-terminal configuration on a Fe/MgO/Si contact of 0.4-μm width, at a negative bias of −700 mV ($I = -0.66$ mA). As indicated, the signal consists of a superposition of a broad and a sharp Hanle peak. Fitting the broad Hanle signal and subtracting that from the measured signal results in the data shown in the inset (symbols). The solid line in the inset is the expected Hanle signal for delocalized electrons in the Si channel, calculated using a spin-relaxation time of 18 ns, as previously determined from nonlocal spin-transport data in the same device. $T = 10$ K.

APPENDIX B

Conforming with previous work [27], we attribute the *existence* of the inverted Hanle effect to the presence of magnetostatic stray fields B^{ms} near the boundary of the ferromagnetic Fe film due to finite roughness, with field components orthogonal to M. However, we attribute the observed shifts and hysteresis of the inverted Hanle curves to the presence of an exchange field B^{exch}, oriented antiparallel to M. One may wonder whether it is possible to explain the data without invoking the exchange field, i.e., can magnetostatic stray fields alone produce the inverted Hanle effect as well as the observed shifts and hysteresis? This scenario can be excluded for two reasons: (i) a shift of the inverted Hanle curve requires a net

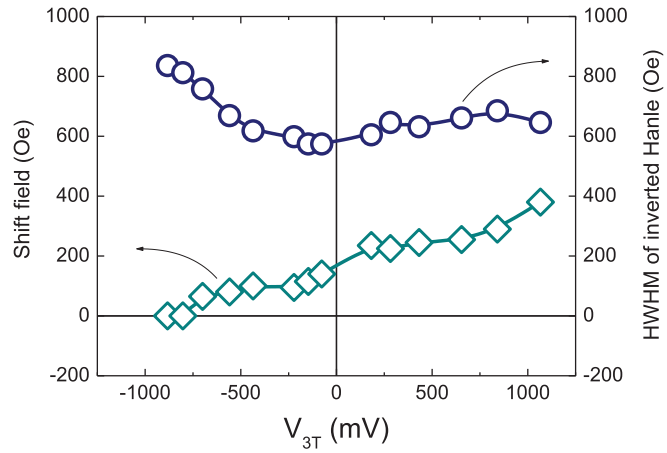

FIG. 6. Half-width at half-maximum (HWHM) of the inverted Hanle spin signal (blue circles), as well as the exchange-induced shift field (green diamonds), as a function of the bias voltage across a Fe/MgO/Si tunnel contact of 0.4-μm width. $T = 10$ K.

nonzero component of the internal field collinear with the magnetization direction, after averaging over the contact area. However, the magnetostatic fields produced by roughness are expected to vary randomly as a function of lateral position, both in magnitude and in direction. It is therefore not likely that roughness produces a net stray field collinear with M, (ii) the magnitude of the observed shift field was found to depend critically on the bias voltage across the tunnel contact (see Fig. 4). Magnetostatic stray fields, however, should be independent of the bias voltage. Indeed, the width of the inverted Hanle curves, which is determined by the magnitude of the stray fields [27], does not depend much on the bias voltage (see Fig. 6). The linewidth is between 600 and 700 Oe for most biases, and slightly larger values are obtained for large negative bias. Notably, whereas the observed shift field decays to zero for increasing negative bias (Fig. 6), the width of the inverted Hanle curve does not. For the largest negative biases, clear inverted Hanle signals still exist and there is no reduction in the linewidth. Hence, the stray fields do not disappear at large negative bias, only the shift field goes to zero. The fact that the width of the inverted Hanle curve and the shift field exhibit completely different variations as a function of the bias voltage is inconsistent with an interpretation in terms of magnetostatic stray fields alone. Hence, two different types of fields must be at play.

Finally, an explanation in terms of a paramagnetic layer at the FM/MgO interface, as previously proposed [34] to explain similar features in the inverted Hanle curves, can be ruled out because it is inconceivable that a sizable nonequilibrium spin accumulation is created within such a paramagnetic layer directly in contact with a FM. The buildup of a spin accumulation would be severely hampered by leakage of the spins into the FM, in which spin relaxation is very efficient. Therefore, the Hanle and inverted Hanle effects are associated with the spin accumulation at the MgO/Si interface, consistent with the fact that the broad Hanle and inverted Hanle signals depend on the semiconductor [29,40] (p or n type, Si or Ge, etc.) and are not observed in Fe/MgO contacts on Ru metal, as long as the tunnel barrier is properly oxidized [40].

[1] N. Tombros, C. Jozsa, M. Popinciuc, H. T. Jonkman, and B. J. van Wees, Electronic spin transport and spin precession in single graphene layers at room temperature, Nature (London) **448**, 571 (2007).

[2] W. Han, R. K. Kawakami, M. Gmitra, and J. Fabian, Graphene spintronics, Nat. Nanotechnol. **9**, 794 (2014).

[3] W. Han, Perspectives for spintronics in 2D materials, APL Mater. **4**, 032401 (2016).

[4] W. Yan, O. Txoperena, R. Llopis, H. Dery, L. E. Hueso, and F. Casanova, A two-dimensional spin field-effect switch, Nat. Commun. **7**, 13372 (2016).

[5] A. Dankert and S. P. Dash, Electrical gate control of spin current in van der Waals heterostructures at room temperature, Nat. Commun. **8**, 16093 (2017).

[6] I. Žutić, A. Matos-Abiague, B. Scharf, H. Dery, and K. Belashchenko, Proximitized materials, Mater. Today **22**, 85 (2019).

[7] H. Haugen, D. Huertas-Hernando, and A. Brataas, Spin transport in proximity-induced ferromagnetic graphene, Phys. Rev. B **77**, 115406 (2008).

[8] Y. G. Semenov, K. W. Kim, and J. M. Zavada, Spin field effect transistor with a graphene channel, Appl. Phys. Lett. **91**, 153105 (2007).

[9] P. Wei, S. Lee, F. Lemaitre, L. Pinel, D. Cutaia, W. Cha, F. Katmis, Y. Zhu, D. Heiman, J. Hone, J. S. Moodera, and C.-T. Chen, Strong interfacial exchange field in the graphene/EuS heterostructure, Nat. Mater. **15**, 711 (2016).

[10] J. Ch. Leutenantsmeyer, A. A. Kaverzin, M. Wojtaszek, and B. J. van Wees, Proximity induced room temperature ferromagnetism in graphene probed with spin currents, 2D Mater. **4**, 014001 (2017).

[11] C. Zhao, T. Norden, P. Zhang, P. Zhao, Y. Cheng, F. Sun, J. P. Parry, P. Taheri, J. Wang, Y. Yang *et al.*, Enhanced valley splitting in monolayer WSe2 due to magnetic exchange field, Nat. Nanotechnol. **12**, 757 (2017).

[12] W. Han, K. Pi, K. M. McCreary, Y. Li, J. J. I. Wong, A. G. Swartz, and R. K. Kawakami, Tunneling Spin Injection into Single Layer Graphene, Phys. Rev. Lett. **105**, 167202 (2010).

[13] M. Gurram, S. Omar, and B. J. van Wees, Bias induced up to 100% spin-injection and detection polarizations in ferromagnet/bilayer-hBN/graphene/hBN heterostructures, Nat. Commun. **8**, 248 (2017).

[14] A. Spiesser, H. Saito, Y. Fujita, S. Yamada, K. Hamaya, S. Yuasa, and R. Jansen, Giant Spin Accumulation in Silicon Nonlocal Spin-Transport Devices, Phys. Rev. Appl. **8**, 064023 (2017).

[15] R. Jansen, A. Spiesser, H. Saito, Y. Fujita, S. Yamada, K. Hamaya, and S. Yuasa, Nonlinear Electrical Spin Conversion in A Biased Ferromagnetic Tunnel Contact, Phys. Rev. Appl. **10**, 064050 (2018).

[16] A. Spiesser, H. Saito, S. Yuasa, and R. Jansen, Tunnel spin polarization of Fe/MgO/Si contacts reaching 90% with increasing MgO thickness, Phys. Rev. B **99**, 224427 (2019).

[17] A. W. Cummings, Probing magnetism via spin dynamics in graphene/2D-ferromagnet heterostructures, J. Phys. Mater. **2**, 045007 (2019).

[18] I. Žutić, J. Fabian, and S. Das Sarma, Spintronics: Fundamentals and applications, Rev. Mod. Phys. **76**, 323 (2004).

[19] J. Fabian, A. Matos-Abiague, C. Ertler, P. Stano, and I. Žutić, Semiconductor spintronics, Acta Phys. Slovaca **57**, 565 (2007).

[20] J. C. Slonczewski, Conductance and exchange coupling of two ferromagnets separated by a tunneling barrier, Phys. Rev. B **39**, 6995 (1989).

[21] J. Faure-Vincent, C. Tiusan, C. Bellouard, E. Popova, M. Hehn, F. Montaigne, and A. Schuhl, Interlayer Magnetic Coupling Interactions of Two Ferromagnetic Layers by Spin Polarized Tunneling, Phys. Rev. Lett. **89**, 107206 (2002).

[22] T. Katayama, S. Yuasa, J. Velev, M. Ye. Zhuravlev, S. S. Jaswal, and E. Y. Tsymbal, Interlayer exchange coupling in Fe/MgO/Fe magnetic tunnel junctions, Appl. Phys. Lett. **89**, 112503 (2006).

[23] L. E. Nistor, B. Rodmacq, S. Auffret, A. Schuhl, M. Chshiev, and B. Dieny, Oscillatory interlayer exchange coupling in MgO

tunnel junctions with perpendicular magnetic anisotropy, Phys. Rev. B **81**, 220407 (2010).

[24] J. C. S. Kools, W. Kula, D. Mauri, and T. Lin, Effect of finite magnetic film thickness on Néel coupling in spin valves, J. Appl. Phys. **85**, 4466 (1999).

[25] B. D. Schrag, A. Anguelouch, S. Ingvarsson, G. Xiao, Y. Lu, P. L. Trouilloud, A. Gupta, R. A. Wanner, W. J. Gallagher, P. M. Rice, and S. S. P. Parkin, Néel "orange-peel" coupling in magnetic tunneling junction devices, Appl. Phys. Lett. **77**, 2373 (2000).

[26] A. Anguelouch, B. D. Schrag, G. Xiao, Y. Lu, P. L. Trouilloud, R. A. Wanner, W. J. Gallagher, and S. S. P. Parkin, Two-dimensional magnetic switching of micron-size films in magnetic tunnel junctions, Appl. Phys. Lett. **76**, 622 (2000).

[27] S. P. Dash, S. Sharma, J. C. Le Breton, J. Peiro, H. Jaffrès, J.-M. George, A. Lemaître, and R. Jansen, Spin precession and inverted Hanle effect in a semiconductor near a finite-roughness ferromagnetic interface, Phys. Rev. B **84**, 054410 (2011).

[28] X. Lou, C. Adelmann, M. Furis, S. A. Crooker, C. J. Palmstrøm, and P. A. Crowell, Electrical Detection of Spin Accumulation at A Ferromagnet-Semiconductor Interface, Phys. Rev. Lett. **96**, 176603 (2006).

[29] S. P. Dash, S. Sharma, R. S. Patel, M. P. de Jong, and R. Jansen, Electrical creation of spin polarization in silicon at room temperature, Nature (London) **462**, 491 (2009).

[30] R. Moubah, F. Magnus, T. Warnatz, G. K. Palsson, V. Kapaklis, V. Ukleev, A. Devishvili, J. Palisaitis, P. O. Å. Persson, and B. Hjörvarsson, Discrete Layer-by-Layer Magnetic Switching in Fe/MgO(001) Superlattices, Phys. Rev. Appl. **5**, 044011 (2016).

[31] F. Magnus, T. Warnatz, G. K. Palsson, A. Devishvili, V. Ukleev, J. Palisaitis, P. O. Å. Persson, and B. Hjörvarsson, Sequential magnetic switching in Fe/MgO(001) superlattices, Phys. Rev. B **97**, 174424 (2018).

[32] C. Cerqueira, J. Y. Qin, H. Dang, A. Djeffal, J.-C. Le Breton, M. Hehn, J.-C. Rojas-Sanchez, X. Devaux, S. Suire, S. Migot *et al.*, Evidence of pure spin-current generated by spin pumping in interface-localized states in hybrid metal-silicon-metal vertical structures, Nanolett. **19**, 90 (2019).

[33] A. Spiesser, H. Saito, R. Jansen, S. Yuasa, and K. Ando, Large spin accumulation voltages in epitaxial Mn_5Ge_3 contacts on Ge without an oxide tunnel barrier, Phys. Rev. B **90**, 205213 (2014).

[34] S. Sato, R. Nakane, and M. Tanaka, Origin of the broad three-terminal Hanle signals in $Fe/SiO_2/Si$ tunnel junctions, Appl. Phys. Lett. **107**, 032407 (2015).

[35] B. Karpiak, A. W. Cummings, K. Zollner, M. Vila, D. Khokhriakov, A. Md. Hoque, A. Dankert, P. Svedlindh, J. Fabian, S. Roche, S. P. Dash, Magnetic proximity in a van der Waals heterostructure of magnetic insulator and graphene, arXiv:1908.05524.

[36] R. Jansen, Silicon Spintronics, Nat. Mater. **11**, 400 (2012).

[37] R. Jansen, S. P. Dash, S. Sharma, and B. C. Min, Silicon spintronics with ferromagnetic tunnel devices, Semicond. Sci. Technol. **27**, 083001 (2012).

[38] V. Sverdlov and S. Selberherr, Silicon spintronics: Progress and challenges, Phys. Rep. **585**, 1 (2015).

[39] M. Tran, H. Jaffrès, C. Deranlot, J.-M. George, A. Fert, A. Miard, and A. Lemaître, Enhancement of the Spin Accumulation at the Interface between A Spin-Polarized Tunnel Junction and A Semiconductor, Phys. Rev. Lett. **102**, 036601 (2009).

[40] S. Sharma, A. Spiesser, S. P. Dash, S. Iba, S. Watanabe, B. J. van Wees, H. Saito, S. Yuasa, and R. Jansen, Anomalous scaling of spin accumulation in ferromagnetic tunnel devices with silicon and germanium, Phys. Rev. B **89**, 075301 (2014).

[41] R. Jansen, A. M. Deac, H. Saito, and S. Yuasa, Injection and detection of spin in a semiconductor by tunneling via interface states, Phys. Rev. B **85**, 134420 (2012).